



HAL
open science

Does roughening of rock-fluid-rock interfaces emerge from a stress-induced instability?

Eric Bonnetier, Chaouqi Misbah, François Renard, Renaud Toussaint, Jean Pierre Gratier

► **To cite this version:**

Eric Bonnetier, Chaouqi Misbah, François Renard, Renaud Toussaint, Jean Pierre Gratier. Does roughening of rock-fluid-rock interfaces emerge from a stress-induced instability?. The European Physical Journal B: Condensed Matter and Complex Systems, 2009, 67 (1), pp.121-131. 10.1140/epjb/e2009-00002-2 . insu-00352886

HAL Id: insu-00352886

<https://insu.hal.science/insu-00352886>

Submitted on 14 Jan 2009

HAL is a multi-disciplinary open access archive for the deposit and dissemination of scientific research documents, whether they are published or not. The documents may come from teaching and research institutions in France or abroad, or from public or private research centers.

L'archive ouverte pluridisciplinaire **HAL**, est destinée au dépôt et à la diffusion de documents scientifiques de niveau recherche, publiés ou non, émanant des établissements d'enseignement et de recherche français ou étrangers, des laboratoires publics ou privés.

Does roughening of rock-fluid-rock interfaces emerge from a stress-induced instability?

E. Bonnetier¹, C. Misbah^{2,a}, F. Renard^{3,4}, R. Toussaint^{5,6}, and J.-P. Gratier³

¹ Laboratoire Jean Kuntzmann, Université Joseph Fourier and CNRS, B.P. 53, 38041 Grenoble Cedex 9, France

² Laboratoire de Spectrométrie Physique, 140 avenue de la physique, Université Joseph Fourier, and CNRS, 38402, Saint Martin d'Hères, France

³ Laboratoire de Géodynamique des Chaînes Alpines, CNRS-OSUG, Université Joseph Fourier, B.P. 53, 38041 Grenoble, France

⁴ Physics of Geological Processes, University of Oslo, Norway

⁵ Institut de Physique du Globe de Strasbourg, UMR CNRS 7516, 5 rue Descartes, 67084 Strasbourg Cedex, France

⁶ EOST, Université de Strasbourg, France

Received 20 October 2008 / Received in final form 24 November 2008

Published online (Inserted Later) – © EDP Sciences, Società Italiana di Fisica, Springer-Verlag 2008

Abstract. Non-planar solid-fluid-solid interfaces under stress are very common in many industrial and natural materials. For example, in the Earth's crust, many rough and wavy interfaces can be observed in rocks in a wide range of spatial scales, from undulate grain boundaries at the micrometer scale, to stylolite dissolution planes at the meter scale. It is proposed here that these initially flat solid-fluid-solid interfaces become rough by a morphological instability triggered by elastic stress. A model for the formation of these unstable patterns at all scales is thus presented. It is shown that such instability is inherently present due to the uniaxial stress that promotes them, owing to the gain in the total elastic energy: the intrinsic elastic energy plus the work of the external forces. This is shown explicitly by solving the elastic problem in a linear stability analysis, and proved more generally without having resort to the computation of the elastic field.

PACS. 91.32.De Crust and lithosphere – 68.35.Fx Diffusion; interface formation – 02.30.Jr Partial differential equations – Plasticity, diffusion, and creep Plasticity, diffusion, and creep – 91.60.Dc Plasticity, diffusion, and creep

1 Introduction

When a solid is non-uniformly loaded (Fig. 1), its elastic free energy is increased and local gradients of free-energy can induce mass transfer from the most stressed sides of the solid to the least stressed ones, or to other surrounding solids, to minimize the energy increase related to the loading. The interface kinetics of the stressed solid is controlled by the slowest mechanism by which the mass is transported. This configuration is found in many layered industrial materials or natural systems. For example, in the rocks of the Earth's crust, loaded interfaces are widespread: fault surfaces and stylolites (Fig. 2) at a macroscopic scale; grain boundaries and grain free surfaces in a porous medium at the microscopic scale.

Two different geometries can be defined, depending on the orientation of the main compressive stress relative to the loaded interface (Fig. 1).

- When the main compressive stress is parallel to the surface, grooves can develop, this is the Asaro-Tiller-Grinfeld instability [3,11,12,21,23,31], referred to, later in this paper, as “the free-face instability”. This instability is well understood theoretically. It has been observed on Helium by Torii and Balibar [33]. It has also been proposed that it could be reproduced experimentally on sodium chlorate single crystals [7]. However, experiments on the same salt do also show that this instability may disappear after some time. This effect might be related to the precipitation of a stress-free skin at the surface of the crystals [5].
- When the main compressive stress is perpendicular to the solid surface, initially flat dissolution surfaces can become rough in the course of time by a dissolution process. Typical natural examples of such squeezed unstable interfaces can be observed in natural rocks. They are called stylolites (Fig. 2). In sedimentary basins, stylolites are observed as rough horizontal interfaces [8,13,24,30,32]. There, the main compressive

^a e-mail: chaouqi.misbah@ujf-grenoble.fr

stress is vertical and corresponds to the weight of the overburden rocks. In mountain chains, where the main compressive stress corresponds to the horizontal tectonic loading, rough stylolite surfaces are oriented vertically [2,25]. From these basic observations, one may conclude that stress is a key ingredient in stylolite pattern formation [4,17]. In the present study, we call such roughening process “the squeezed interface instability”. It differs from the free-face instability by the orientation of the main compressive stress. This second instability is less understood. It has been proposed that the roughening of the interface is controlled by a destabilizing force, the noise initially present in the rock [26,27]. In [9] it was assumed that diffusion occurs along the solid-solid interface and a simple model to describe the instability has been proposed. However, a model that takes into account a more realistic geometry is lacking, together with a systematic derivation of the governing equations. Furthermore, it remains to be shown whether or not a purely elastic instability explains the formation of stylolites. This paper is directed along these lines.

We present a model that shows that squeezed solid-fluid interfaces are unstable due to stress. This situation is less classical than the one usually treated: here two solids are in contact with a thin liquid layer and the weight is transmitted from one solid to the other by the liquid layer. It is thus essential to derive the equations and boundary conditions in this geometry. We must take into account not only the intrinsic elastic energy but also the work due to external forces.

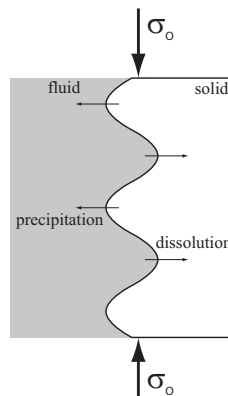
Natural and experimental observations of rough surfaces indicate that stress has a strong control on the evolution of the fluid-solid interfaces: stress gradients are released by dissolution-precipitation or melting solidification processes, which modify the solid texture and induce irreversible deformations (see Fig. 2).

The scheme of this paper is as follows. In Section 2 we briefly review the free interface case. In Section 3 we treat the squeezed interface case by performing a linear stability analysis, and present the main results that reveals an instability driven by stress. In Section 4 we present a more general and formal proof of the instability without having resort to an explicit solution of the elastic field. Section 5 is devoted to a general discussion. Some technical details are presented in an appendix.

2 The free interface case

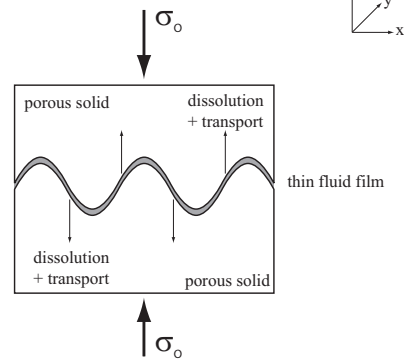
If the main compressive stress is parallel to the loaded interface (Fig. 1a), grooves can develop on the free surface. This is the well-known Asaro-Tiller-Grinfeld instability [3,11]. It has been found experimentally [7,19,33] that the formation of the grooves occurs on a free surface of various solids in contact with a fluid when a load (or a uniaxial stress [33]) is applied. The grooves can theoretically evolve to fractures that propagate at a subcritical rate [14,16,18,31,34]. The wavelength of the instability

free surface instability



a)

stylolite instability



b)

Fig. 1. Morphological instabilities of a solid-fluid interface and effect of the orientation of the main compressive stress. (a) Free-face instability: when a free surface of a solid in contact with a fluid is loaded perpendicular to the surface, grooves can develop through time and even evolve to cracks. This is the Asaro-Tiller-Grinfeld instability. (b) Squeezed interface instability: A typical example is a stylolite, which corresponds to a fluid-filled rock-rock interface loaded perpendicularly to the interface. The mean roughness amplitude of the interface grows with time, which gives their characteristic shapes to the stylolites. In both cases, the fluid phase acts as a reactive medium transporting solutes by diffusion and allowing stress driven dissolution-precipitation processes at the interface with the solid.

is controlled by a balance between elastic forces, which tend to roughen the surface, and surface tension, which smoothen it. The characteristic wavelength λ_c of the instability that emerges from a linear stability analysis is

$$\lambda_c = \frac{\pi E \gamma}{\sigma_0^2 (1 - \nu^2)}, \quad (1)$$

where E is the Young modulus of the solid, γ is the interfacial energy between the solid and the liquid, ν is the Poisson coefficient, and σ_0 is the applied main compressive stress (see Fig. 1). The planar front is unstable if the perturbation wavelength λ is such that $\lambda > \lambda_c$ and it is stable otherwise.

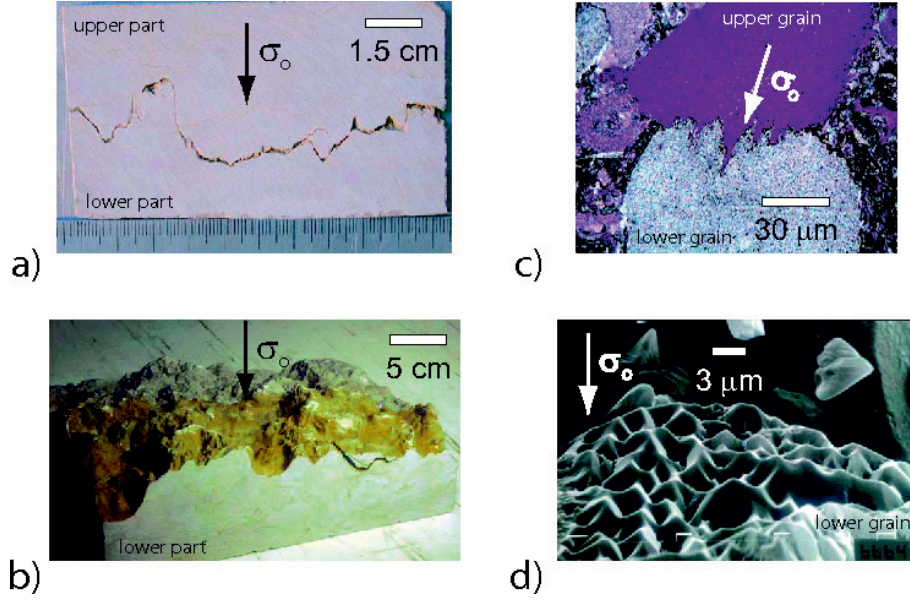


Fig. 2. Various patterns of rough stylolite interfaces at all scales. (a) Stylolite interface in a sedimentary limestone from the Chartreuse Mountains, France. The rough interface pattern formed by stress-enhanced dissolution from an initially flat rock-fluid-rock interface. In this case, the maximum compressive stress σ_0 was perpendicular to the interface. (b) Stylolite surface viewed in 3D after removing the upper part of a limestone, similar to the sample shown in (a). (c) Microscopic observation of a rough grain-grain boundary in a limestone from Mons, Belgium, showing two spherical grains indented into each other. The rough teeth pattern of the interface has formed by a stress-enhanced dissolution process. (d) Scanning Electron Microscope view of a quartz grain surface, after experimentally produced stress-enhanced dissolution against a second quartz grain that has been removed for better visualization. The maximum stress was vertical, and perpendicular to the rough interface. Adapted from [10].

1 For the case of rocks, in which we are interested here,
 2 it has been shown that the transport mechanism may be
 3 controlled either by dissolution kinetics of the crystal, or
 4 diffusion of solutes in the fluid [9,21]. This depends on the
 5 nature of rocks, as discussed in [21].

6 3 The squeezed interface case

7 3.1 Presentation of the instability

8 Consider the situation depicted in Figure 3, where the
 9 initial surface representing the position of the squeezed
 10 interface Γ is set at $z = 0$. The interface contains a thin
 11 water film at a pressure p , squeezed between the two solids
 12 that have identical linear elastic properties. We consider,
 13 for the sake of simplicity, one dimensional deformations
 14 along x only, so that the stress and the strain fields are
 15 independent of y . Here we shall not describe the mecha-
 16 nisms by which the modulation takes place, but, rather,
 17 we are interested to compare the energetic of the initial
 18 state (flat) with that of a corrugated one.

19 Due to the assumption of translational invariance
 20 along y , the problem reduces to an effective 2D one where
 21 it is convenient to make use of the Airy function $\chi(x, z)$
 22 which is defined in terms of the stress tensor as [20]:

$$\sigma_{xx} = \frac{\partial^2 \chi}{\partial z^2}, \sigma_{zz} = \frac{\partial^2 \chi}{\partial x^2}, \sigma_{xz} = -\frac{\partial^2 \chi}{\partial x \partial z}. \quad (2)$$

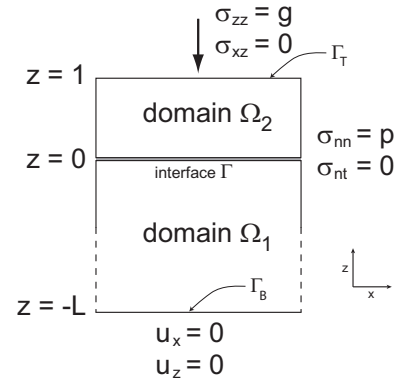


Fig. 3. Geometry of the system: two linear elastic solids with identical moduli are pushed into each other and separated by a thin confined water film at pressure p . The boundaries conditions used in Sections 3 and 4 are given.

The Airy function χ obeys a bi-harmonic equation [20]:

$$\nabla^4 \chi = 0. \quad (3)$$

24 Once χ is determined the stress can be computed from
 25 the very definition of χ , and the strain is obtained from
 26 Hooke's law. It must be emphasized that since we confine
 27 ourselves to two dimensional deformations, the strain-
 28 stress relation differs from the three dimensional version
 29 (as far as the coefficients are concerned). We have in two

1 dimensions the relations

$$\begin{aligned}\varepsilon_{xx} &= \frac{1+\nu}{E}[(1-\nu)\sigma_{xx} - \nu\sigma_{zz}] \\ \varepsilon_{zz} &= \frac{1+\nu}{E}[(1-\nu)\sigma_{zz} - \nu\sigma_{xx}] \\ \varepsilon_{xz} &= \frac{1+\nu}{E}\sigma_{xz}\end{aligned}\quad (4)$$

2 where E is the Young's modulus of the solid and ν is the
3 Poisson's ratio. This limit is also known as the plane strain
4 condition.

5 The interface equation is written as $z = h(x)$. For
6 $h = 0$, $\chi_0 = gx^2/2$ (the subscript '0' refers to the planar
7 interface) is obviously a solution of (3) with $\sigma_{zz} = g$
8 the only non zero component. This solution satisfies the
9 boundary condition at $z = 1$, and from $\sigma_{nn} = p$, we obtain
10 $p = g$. This is physically appealing since the equilibrium
11 at the interface, where the force is normal and equal to p ,
12 requires a compensation of the applied load g . Apart from
13 a hydrostatic pressure (taken as an origin), both $\sigma_{xx} = 0$
14 and $\sigma_{xz} = 0$. The pre-strained situation is uniaxial.

15 Let us now assume that the interface undergoes a virtual
16 displacement $h(x)$ and compute the resulting elastic
17 fields in both solid domains denoted as '1' and '2'. Of
18 course in its great generality this problem is highly non-
19 linear for an arbitrary h , and can only be dealt with numerically.
20 If one is interested in determining whether or
21 not an interface displacement results in a gain of energy,
22 it may be sufficient to perform a linear stability analysis,
23 a problem which can be handled analytically.

24 Because different modes do not interact in the linear
25 regime, it is sufficient to consider only one Fourier component,
26 namely we seek solutions in the form:

$$h = \varsigma e^{iqx} + c.c. \quad (5)$$

27 where ς is a small parameter, small enough for a linear
28 analysis to make a sense, and q is the perturbation
29 wavenumber. The perturbed Airy function can also be decomposed
30 onto Fourier modes

$$\chi = \varsigma f(z) e^{iqx} + c.c. + \chi_0 \quad (6)$$

31 where f is a function which is yet unknown. From (3) it
32 follows that f obeys

$$\left[\frac{\partial^2}{\partial z^2} - q^2 \right]^2 f = 0. \quad (7)$$

33 The general solution of which reads

$$f = (Az + B)e^{qz} + (A'z + B')e^{-qz}. \quad (8)$$

34 The four integration factors A, A', B, B' are computed
35 from the boundary conditions.

36 In domain '1' (lower domain) we have

$$f = (A_1z + B_1)e^{qz} + (A'_1z + B'_1)e^{-qz}. \quad (9)$$

37 In domain '2' we have

$$f = (A_2z + B_2)e^{qz} + (A'_2z + B'_2)e^{-qz}. \quad (10)$$

The eight integration factors are determined by the eight
38 conditions: the normal stress at $z = 1$ is equal to g where
39 the surface there is free from shear. These two conditions
40 read

$$\sigma_{zz}|_{z=1} = g, \quad \sigma_{xz}|_{z=1} = 0. \quad (11)$$

42 At the interface the normal components on both sides
43 coincide with p , while the tangential components vanish.
44 This amounts to four independent conditions

$$\begin{aligned}\sigma_{nn}|_{z=0^-} &= p, & \sigma_{nn}|_{z=0^+} &= p, \\ \sigma_{nt}|_{z=0^-} &= 0, & \sigma_{nt}|_{z=0^+} &= 0\end{aligned}\quad (12)$$

45 where $\sigma_{nn} = n_i \sigma_{ij} n_j$ and $\sigma_{nt} = n_i \sigma_{ij} t_j$, with n_i and t_j
46 representing the i^{th} component of the normal and the tangential
47 vectors evaluated at the interface. Note that from zeroth order
48 solution we have seen that $p = g$, so that from now on we shall
49 abandon the p symbol in favor of g .

50 Finally at the bottom, $z = -L$, we impose a zero displacement
51 condition, namely

$$u_z|_{z=-L} = 0, \quad u_x|_{z=-L} = 0. \quad (13)$$

52 Using the Airy function and the definition (2) together
53 with (9) and (10), and expanding the equations to order
54 one in ς we obtain eight equations determining the eight
55 unknowns. The solutions take the form

$$\begin{aligned}A_1 &= g[e^{-2qL}(2qL + 1) + 3 - 4\nu]/D_1 \\ B_1 &= 2ge^{-2qL}[q^2L^2 + 2 + 4\nu^2 - 6\nu]/D_1 \\ A'_1 &= ge^{-2qL}[1 - 2qL + e^{-2qL}(3 - 4\nu)]/D_1 \\ B'_1 &= -B_1 \\ A_2 &= -g[e^{2q}(2q - 1) + 1]/D_2 \\ B_2 &= 2qge^{2q}/D_2 \\ A'_2 &= -ge^{2q}[e^{2q} - 2q - 1]/D_2 \\ B'_2 &= -2qge^{2q}/D_2\end{aligned}\quad (14)$$

56 where we have set

$$D_1 = (3 - 4\nu)[1 + e^{-4qL}] + 2e^{-2qL}[2q^2L^2 + 8\nu^2 - 12\nu + 5] \quad (15)$$

and

$$D_2 = 2e^{2q}(2q^2 + 1) - 1 - e^{4q}. \quad (16)$$

58 Having determined these eight constants of integration,
59 the elastic field can be obtained straightforwardly.

3.2 Energy considerations

60 In this section we will be mainly concerned with the total
61 energy of the system in the deformed and undeformed
62 states. The total energy should contain both the intrinsic
63 part and the work of the external force, g . The energy
64 contribution from the intrinsic part is $1/2 \int_{\Omega} \sigma d\tau : \varepsilon(u)$
65 where Ω is the total volume, and the work of the external
66 force is $-\int_{\Gamma_T} gu$, with Γ_T is the upper boundary (see
67 Fig. 3). The total energy is thus

$$E = \frac{1}{2} \int_{\Omega} \sigma : \varepsilon(u) d\tau - \int_{\Gamma_T} gu. \quad (17)$$

It will be shown in Section 4 that minimization of this energy with respect to u yields the appropriate elastic equations, $\text{div}(\sigma) = 0$ and the boundary conditions (11), (12), and (13). Upon substitution of the equilibrium condition, the relaxed elastic energy will then take the following form

$$E_0 = -\frac{1}{2} \int_{\Omega} \sigma : \varepsilon(u) d\tau \quad (18)$$

where the subscript ‘0’ is to remind us that the quantity under consideration is the relaxed energy. That this quantity is negative is obvious, since the relaxed energy should be smaller than the non-relaxed one, otherwise there is a trivial solution which would have a zero energy, the one corresponding to a zero displacement.

It remains now to be shown that the variation of this quantity with respect to an interface modulation $\varsigma \cos(qx)$ (produced due to some mass transport) is negative, a signature of the instability. A general proof is presented in Section 4 without resorting to the explicit form of the elastic field. It is also of interest to have an explicit expression of the energy, (and possibly of the chemical potential), if one wishes to study the kinetics of the instability, and provide the appropriate length and time scales of the evolution.

We should remind that σ has a zeroth order contribution due to pre-strain, and in computing the energy E_0 one has to subtract the energy of the pre-strained state, so that the obtained form contains the contribution due to the profile $z = h(x, t)$. In the linear regime of perturbation with respect to h (i.e. the stress is computed up to order h), the energy E_0 assumes a quadratic form. In the general situation where the extent of the upper and lower parts of the sample is finite the energy is lengthy enough so we did not feel it worthwhile to list it here. We give only the limit where $qL \gg 1$ (lower part, below the interface, is large in comparison to lengths of interest):

$$E_0 = qg^2 \frac{1+\nu}{ED_2} \left\{ (1-2\nu) [1 + e^{4q} - 2e^{2q} - 4q^2 e^{2q}] - 4qe^{2q} + e^{4q} - 1 \right\} \varsigma^2 \quad (19)$$

where D_2 is a constant defined in equation (16). The above energy is computed per unit period along x and per unit length along y . If the surface energy (39) is taken into account, one has to supplement E_0 with the following contribution

$$E_s = \gamma \int dx \left(\frac{dh}{dx} \right)^2 \quad (20)$$

where we have used the approximation of small perturbation so that the change of arclength from the planar surface configuration is approximated by $(dh/dx)^2$. The cost in surface energy per unit period and unit length in the y direction is thus given by

$$E_s = \gamma q^2 \varsigma^2. \quad (21)$$

It can be checked that the right hand side in equation (19) is always negative, signaling an instability. Note that if the work of the external forces in (17) is not included, then

the relaxed energy would be the opposite of (18), and therefore E_0 would have been positive in equation (19), signaling a stability instead of instability. This will further be shown in the general treatment in Section 4. In contrast to elasticity, the surface energy is stabilizing. A remark is in order. The comparison of the elastic energy (which is destabilizing) and the surface energy (which is stabilizing) has also a similar spirit as that due Griffith in fracture theory. Indeed, in Griffith theory a crack propagates if its length ℓ exceeds a typical value given by the ratio of the loss of surface energy γ over the gain in elastic energy (crack releases stored elastic energy) $\sim \sigma_0^2/E$. More interesting is that the Griffith condition, according to which a crack propagates when its length exceeds a critical length ℓ_c , is precisely (apart from a numerical factor of order unity) the condition of the ATG instability: the planar front is unstable if the wavelength is larger than λ_c (see Eq. (1)), whereas the Griffith condition states [20] that a crack propagates if its length $\ell > \ell_c = (4/\pi^2)\lambda_c$.

We shall first discuss the two extreme limits of large and short wavenumbers. In these extreme limits the expression takes a very simple form. The first case is, perhaps, the most relevant one for natural systems such as stylolites, where we assume that $q \gg 1$ (short wavelength). This means that we take the limit where the modulation wavelength is small as compared to the interface extent. The energy (per unit period) takes then the form

$$E_0 = -\frac{4(1-\nu^2)}{E} |q| g^2 \varsigma^2 \quad (22)$$

which is negative, signaling a morphological instability. Note that we keep $|q|$ in the expression above in order to stress the nonlocal character of the elastic field. Indeed, in real space the quantity $|q|$ leads to a Hilbert transform of $\partial_x h(x)$. More precisely

$$TF^{-1}(|q|h_q) = (1/\pi) \mathcal{P} \int \frac{\partial_{x'} h(x')}{x' - x}, \quad (23)$$

where TF stands for a Fourier transform, and $h_q = TF^{-1}(h)$ (TF^{-1} designates the inverse Fourier transform). The symbol \mathcal{P} refers to the fact that the integral must be taken in the sense of the Cauchy principal value. For a real function $f(x)$ the Cauchy principal value is defined as

$$\mathcal{P} \int_{-\infty}^{\infty} \frac{f(x)}{x} dx \equiv \lim_{\epsilon \rightarrow 0} \left[\int_{-\infty}^{-\epsilon} \frac{f(x)}{x} dx + \int_{\epsilon}^{\infty} \frac{f(x)}{x} dx \right]. \quad (24)$$

Let us abbreviate this expression as $pv(f(x)/x)$. Applying TF on both sides of (23), one gets on the left hand side $|q|h_q$, while the right hand side is a convolution providing a product of $TF(\partial_{x'} h(x'))$ and $TF(pv(1/(x' - x)))$. The first term yields iqh_q , while the second one is equal to $-i\pi \text{sgn}(q)$ (a classical result of theory of distributions, and can easily be obtained by using the residue theorem), $\text{sgn}(q)$ stands for ‘sign of q ’. The final result (after accounting for the factor π in (23)) is $q \text{sgn}(q) h_q = |q|h_q$, that is identical to the left hand side result.

In the opposite limit ($q \ll 1$) one gets (for $L = 1$)

$$E_0 = -\frac{2(1+\nu)}{15E(1-\nu)}g^2q^2(17-32\nu)\zeta^2. \quad (25)$$

The effect of the confinement leads to a spectrum which begins with q^2 instead of q . This may have, in principle, some significant consequences, as discussed below.

For example, in the non-confined regime the elastic energy (which is $\sim q$) dominates at small q in comparison to the surface energy which behaves as q^2 . This means that the instability is always present there. The typical length-scale of the instability is given by balancing the elastic energy $\sim qg^2/E$ with the surface energy $\sim \gamma q^2$ where γ is the surface energy. This leads to a typical length scale $\lambda_c \sim E\gamma/g^2$.

In the confined regime the energy behaves as $-q^2g^2\ell E$ (where for homogeneity reasons we have reintroduced a length scale ℓ representing a typical length of the vertical extent of the solid), precisely like the surface energy regarding the q dependence, $+q^2\gamma$. Since the latter is stabilizing, while the former is destabilizing, an instability may take place only if $\ell > \gamma E/g^2$. g has a dimension of E and can be written as $g = nE$ where n is a dimensionless number smaller than one. We must have then $\ell > \gamma/(nE)$. In most cases γ/E is of the order of an atomic length and n is small enough so we conclude that for all practical purposes the instability takes place.

4 A general framework

In this section, we cast the previous calculation in the framework of a variational analysis. We provide a rigorous mathematical derivation on the stress-induced instability. Unlike the previous derivation, the present result will be obtained without knowing the explicit expression of the elastic field. We restrict ourselves to a 2D situation for simplicity; however, the analysis carries over to the 3D case. We consider a configuration similar to that of Figure 3: a portion of interface Γ separates two pieces of solids Ω_1 and Ω_2 in the rectangle $\Omega = \Omega_1 \cup \Omega_2 \cup \Gamma$.

4.1 Mechanical equilibrium for a fixed interface Γ

We view the rectangle $\Omega = (0, 1) \times (0, 1)$ as a small slab of solid around an interface and assume periodic boundary conditions on the vertical sides $\Gamma_V = \{0\} \times (0, 1) \cup \{1\} \times (0, 1)$. We assume that Ω_1 lies below Ω_2 and that both are sufficiently regular open sets (say with Lipschitz boundaries). A vertical load with modulus g is applied to the top boundary Γ_T and the displacement u_1 is fixed on the bottom boundary Γ_B . We use the Einstein summation convention of repeated indices.

The transmission conditions between Ω_1 and Ω_2 models the presence of a very thin layer of fluid in the interface. We assume therefore that the stress tensors σ_1 and σ_2 in Ω_1 and Ω_2 satisfy

$$\sigma_i n_i = p n_i, \quad \text{on } \Gamma, \quad i = 1, 2,$$

where n_i denotes the outward normal to Ω_i , and where p is the Lagrange multiplier that denotes the (unknown) pressure in the thin layer of fluid. Altogether, the mechanical equilibrium of the system is expressed by the equations

$$\begin{cases} -\operatorname{div}(\sigma_i) = 0 & \text{in } \Omega_i, \\ \sigma_i & = A\varepsilon(u_i) & \text{in } \Omega_i, \\ \sigma_2 n_2 & = g n_2 & \text{on } \Gamma_T, \\ u_1 & = 0 & \text{on } \Gamma_B, \\ u_i & \text{periodic on } \Gamma_V, \\ \sigma_i n_i & = p n_i & \text{on } \Gamma, \end{cases} \quad (26)$$

where $i = 1, 2$, $\varepsilon(u) = 1/2(\nabla u + \nabla u^T)$ is the symmetric strain tensor, and A is the 4×4 tensor of isotropic Lamé coefficients of the solid. Alternatively, the above partial differential equations can be obtained as the Euler Lagrange equations of the following energy functional

$$E_\Gamma(v_1, v_2) = \frac{1}{2} \int_{\Omega_i} A\varepsilon(v_i) : \varepsilon(v_i) dx - \int_{\Gamma_T} g n_2 v_2. \quad (27)$$

The set V of admissible displacements V_Γ consists of pairs $(v_1, v_2) : \Omega_1 \times \Omega_2 \rightarrow \mathbf{R}^2 \times \mathbf{R}^2$ of square integrable functions, with square integrable derivatives, such that

$$\begin{cases} v_1 = 0 & \text{on } \Gamma_T \\ v_1, v_2 & \text{periodic on } \Gamma_V \\ \int_{\Gamma} v_1 n_1 + v_2 n_2 = 0. \end{cases} \quad (28)$$

Note that the constraint on the normal displacements on Γ is associated with the Lagrange multiplier p introduced above. One easily checks that minimizing E_Γ over V_Γ yields a solution (u_1, u_2) to the corresponding Euler-Lagrange equation (26), which is defined up to a horizontal translation of u_2 . To obtain a well-defined solution we further impose the normalization condition

$$\int_{\Gamma_T} u_2 \begin{pmatrix} 1 \\ 0 \end{pmatrix} = 0.$$

4.2 First variation with respect to the interface Γ

In this paragraph, we compute the shape derivative, with respect to variations of the interface Γ , of the elastic energy functional

$$J(\Gamma) = \min_{(v_1, v_2) \in V(\Gamma)} E_\Gamma(v_1, v_2).$$

Denoting (u_1, u_2) the solution of the above variational problem (the actual elastic displacements for the geometry defined by the interface Γ , under the loading g) using (26), and integrating by parts shows that

$$\begin{aligned} J(\Gamma) &= \frac{1}{2} \int_{\Omega_i} A\varepsilon(u_i) : \varepsilon(u_i) dx - \int_{\Gamma_T} g n_2 u_2 \\ &= -\frac{1}{2} \int_{\Omega_i} A\varepsilon(u_i) : \varepsilon(u_i) \end{aligned} \quad (27)$$

$$= -\frac{1}{2} \int_{\Gamma_T} g n_2 u_2. \quad (28)$$

To differentiate the functional with respect to variations of the shape of Γ , we follow the approach of Murat and Simon [22,28] which we now briefly recall: Consider perturbations of an open set $\omega \subset \mathbf{R}^2$ of the form

$$\omega_t = \omega + t\theta,$$

where $\theta : \mathbf{R}^2 \rightarrow \mathbf{R}^2$ is a sufficiently smooth function, and t is a small real parameter (the limit $t \rightarrow 0$ will be taken eventually).

Let z be a smooth function and consider the functionals, defined respectively as a volume integral and a surface integral

$$\begin{aligned} J_1(\omega) &= \int_{\omega} z(u) \\ J_2(\omega) &= \int_{\partial\omega} z(u), \end{aligned}$$

where u is the solution of a partial differential equation $Au = 0$ in ω , with boundary conditions $Bu = 0$. The shape derivatives (or functional derivatives) of J_1, J_2 in the direction θ are defined by

$$J'_i(\omega)\theta = \lim_{t \rightarrow 0} \frac{J_i(\omega + t\theta) - J_i(\omega)}{t}.$$

When ω and u are sufficiently smooth, one can show that $J_i(\omega + t\theta) = J_i(\omega) + tJ'_i(\omega)\theta + o(t\|\theta\|)$, and further, that

$$J'_1(\omega)\theta = \int_{\omega} \partial_u z(u) u' + \int_{\partial\omega} z(u) \theta n, \quad (29)$$

$$\begin{aligned} J'_2(\omega)\theta &= \int_{\partial\omega} \partial_u z(u) u' \\ &+ \int_{\partial\omega} [Hz(u) + \partial_n z(u)] \theta n, \end{aligned} \quad (30)$$

where $\partial_n f(x) = \nabla f(x)n$ is the normal derivative of f . The presence of the mean curvature H on $\partial\omega$ in the derivative of the surface integral J_2 results from taking variations of the surface measure. In these expressions, the local derivative u' of u at $x \in \omega$ is defined by

$$u'(x) = \lim_{t \rightarrow 0} \frac{u_t(x) - u(x)}{t},$$

where u_t is the solution to $Au = 0$ in ω_t with the boundary conditions $B_t u_t = 0$.

In our context, we consider perturbations (Ω_1, Ω_2) of the form

$$\Omega_i^t = \Omega_i + t\theta(x, y), \quad i = 1, 2,$$

where $\theta : \mathbf{R}^2 \rightarrow \mathbf{R}^2$ is sufficiently smooth. We assume that θ leaves the outer boundary $\partial\Omega$ fixed, (i.e., θ only modifies the shape of the interface) and that it preserves the volume of each subdomain Ω_i

$$\begin{cases} \theta(x, y) = 0 & \text{on } \partial\Omega \\ |\Omega_i^t| = |\Omega_i| & i = 1, 2, \end{cases} \quad (31)$$

which imposes that

$$\int_{\Gamma} \theta n_i = 0. \quad (32)$$

Let (u_1^t, u_2^t) denote the solution to (26) for the configuration Ω_i^t

$$\begin{cases} \operatorname{div}(Ae(u_i^t)) = 0 & \text{in } \Omega_i^t \\ u_1^t = 0 & \text{on } \partial\Omega_i \cap \Gamma_B \\ A\nabla u_2^t n_2 = g n_2 & \text{on } \Gamma_T \\ u_i^t & \text{periodic on } \Gamma_V \\ Ae(u_i^t) n_i^t = p_t n_i^t, & \text{on } \Gamma + t\theta. \end{cases} \quad i = 1, 2. \quad (33)$$

The local derivatives (u'_1, u'_2) satisfy

$$\operatorname{div}(Ae(u'_i)) = 0 \quad \text{in } \Omega_i \quad (34)$$

and are periodic on the sides Γ_V . The boundary condition (26.d) implies that $u'_1 + \theta_n \partial_n u_1 = 0$ on Γ_B , which, given the hypothesis on θ , reduces to

$$u'_1 = 0 \quad \text{on } \Gamma_B. \quad (35)$$

In the Appendix, we derive the expression of the shape derivative of $J(\Gamma)$. If $\Gamma \subset (0, 1) \times (0, 1)$ is a periodic simple curve, sufficiently smooth, one obtains

$$\begin{aligned} J'(\Gamma)\theta &= \frac{1}{2} \int_{\Gamma} [A\varepsilon(u_1) : \varepsilon(u_1) - A\varepsilon(u_2) : \varepsilon(u_2)] \theta n_1 \\ &- \int_{\Gamma} p [\operatorname{div}(u_1) - \operatorname{div}(u_2)] \theta n_1. \end{aligned} \quad (36)$$

In particular, if Γ is the flat interface $\Gamma^0 = (0, 1) \times \{y_0\}$, the associated displacements are linear:

$$u_i(x, y) = (0, \frac{g}{\lambda + 2\mu} y), \quad i = 1, 2.$$

This greatly simplifies the computations (for instance all the terms on Γ_0 involving curvature vanish) and one finds in (36) that $J'(\Gamma_0)\theta = 0$ for any θ , i.e., the flat interface is a local extremum of the elastic energy functional J . We show below that the sign of the second derivative of J with respect to the interface shape variation tells if the extremum is a minimum or a maximum of the energy functional.

4.3 Second variation with respect to Γ

With the notations of the previous section, the second derivative (with respect to the interface shape variation) of a volume integral is given by [29]

$$\begin{aligned} J''_1(\omega, \theta, \theta) &= (J'_1)'(\omega, \theta, \theta) - J'_1(\omega)(\nabla\theta)\theta \\ &= \lim_{t \rightarrow 0} \frac{J'_1(\omega + t\theta)\theta - J'_1(\omega)\theta}{t} - J'_1(\omega)(\nabla\theta)\theta. \end{aligned}$$

If ω and θ are sufficiently smooth, Simon [29] has shown that

$$\begin{aligned} J_1(\omega + t\theta) &= J_1(\omega) + tJ'_1(\omega)\theta \\ &+ \frac{t^2}{2} J''_1(\omega, \theta, \theta) + o(t^2\|\theta\|). \end{aligned}$$

1 For our objective functional in the form $J(\Gamma) =$
 2 $-1/2 \int_{\Omega_i} A\varepsilon(u_i) : \varepsilon(u_i)$, calculations similar to those pre-
 3 sented in the Appendix show that at $\Gamma = \Gamma^0$

$$J''(\Gamma_0, \theta, \theta) = -2 \int_{\Omega_i} A\varepsilon(u'_i) : \varepsilon(u'_i), \quad (37)$$

4 which is negative, since the elastic densities $A\varepsilon(u'_i) : \varepsilon(u'_i)$
 5 are quadratic and positive, and since the fields u'_i do not
 6 vanish identically. We can thus conclude that when t is
 7 small enough

$$J(\Gamma_0 + t\theta) = J(\Gamma_0) + J'(\Gamma_0)\theta + J''(\Gamma_0, \theta, \theta) + O(\|\theta\|^2) \\ < J(\Gamma_0).$$

10 In other words, any variation away from the flat inter-
 11 face decreases the value of the total elastic energy, which
 12 demonstrates the instability of the flat interface. Had we
 13 disregarded the work due to the external force g in equa-
 14 tion (27), we would then have obtained an opposite sign
 15 (namely $+1/2 \int_{\Omega_i} A\varepsilon(u_i) : \varepsilon(u_i)$) for the relaxed energy, and
 16 thus stability would have been implied.

17 Finally if the boundary conditions at the bottom sur-
 18 face were different, we may ask the question regarding
 19 sensitivity of our conclusion. If, instead of imposing a zero
 20 displacement at the bottom surface, we apply a fixed load,
 21 as for the upper surface, the conclusion about stability is
 22 unchanged. Let us call h the load, then one has to add
 23 to (27) the following term $-\int_{\Gamma_B} hn_1 v_1$, then following ex-
 24 actly the same manipulations as with the last term in (27)
 25 we arrive at the same final conclusion (37). It would be in-
 26 teresting to investigate in the future more general bound-
 27 ary conditions in order to extract the generic conditions
 28 that trigger an instability.

29 5 Discussion

30 5.1 Effect of external work on the calculation 31 of the total energy

32 A point which is worth mentioning is that in writing the
 33 total energy, we must include both the intrinsic elastic
 34 energy and the work due to the external forces. Careless-
 35 ness (for example not including the work done by surface
 36 forces) would be penalized by a fallacious conclusion: the
 37 surface would be stable! A simple argument that the ex-
 38 ternal forces must be included is that when we perform a
 39 variation of the energy with the respect to the displace-
 40 ment field we must arrive to the appropriate bulk (Lamé
 41 equation) and boundary conditions, otherwise, the consid-
 42 ered equations would not fulfill mechanical equilibrium.
 43 This requirement has guided our considerations.

44 5.2 Kinetics effects

45 By comparing the final state to the initial one, we did
 46 not include, *de facto*, explicitly the notion of kinetics. It is

quite clear that two mechanisms play a major role: disso-
 lution and diffusion in the fluid interstices. This has been
 treated for the free surface case where it has been shown
 that both dissolution and diffusion may be limiting fac-
 tors for rocks [21]. We are planning to include diffusion in
 the fluid layer, and due to the thin fluid layer, it is likely
 that diffusion should have a two dimensional character
 (i.e. like surface diffusion; the diffusion constant should
 then be renormalized by the fluid layer). We expect the
 spectrum for the surface fluctuation of diffusion to scale
 like $D\ell^2 q^4$, where ℓ is the fluid thickness, and D is the
 bulk diffusion constant in the liquid. By comparing to the
 usual diffusion limited spectrum Dq^2 , the effective diffu-
 sion should be lowered by a factor of the order of $q\ell \ll 1$
 (wavelengths of stylolites are usually much bigger than the
 fluid thickness).

For example, it has been found in [21] for quartz and
 other rocks that the dissolution is the slowest mechanisms.
 Now due to the thin fluid layer, we expect diffusion to
 compete, if not to limit, the instability. We hope to report
 along these lines in the near future.

5.3 Chemical potential considerations

We translate now the energy calculations performed in
 the previous sections in terms of chemical potential, for
 the sake of future kinetic calculations. The chemical po-
 tential of a solid element at the interface is obtained from
 the energy change with respect to the interface variation.
 This corresponds to the cost in energy that is needed to
 create a bump (a volume element) on the interface. More
 precisely, let E_T denote the sum of the elastic and sur-
 faces energies, then the very definition of the change of
 the chemical potential is

$$\Delta\mu_T = -\frac{\delta E_T}{\delta V} \quad (38)$$

where δ denotes the functional derivative (derivative with
 respect to the interface shape variation). Since we limit
 ourselves to a one dimensional interface, the functional
 derivative corresponds to variation with respect to the in-
 terface profile $h(x)$. It follows that the added (or removed)
 volume element becomes an area element given by $\delta h dx$,
 where dx is a fixed interval along the x direction. Thus
 the chemical potential will be just proportional to $-\frac{\delta E_T}{\delta h}$.
 The surface energy per unit length along the y direction
 reads

$$E_s = \gamma \int \left(\left[1 + \left(\frac{dh}{dx} \right)^2 \right]^{1/2} - 1 \right) dx \quad (39)$$

and its variation with respect to the profile $h(x)$ is given
 by

$$\delta E_s = -\gamma \int \frac{d}{dx} \left(\frac{\frac{dh}{dx}}{\left[1 + \left(\frac{dh}{dx} \right)^2 \right]^{1/2}} \right) dx = -\gamma \int \kappa dx \delta h \quad (40)$$

1 where we have set

$$\kappa = -\frac{\frac{d^2h}{dx^2}}{\left[1 + \left(\frac{dh}{dx}\right)^2\right]^{3/2}} \quad (41)$$

2 which is nothing but the interface curvature. It follows
3 that the contribution to the chemical potential from sur-
4 face energy is given by

$$\Delta\mu_s = -\frac{\delta E_T}{\delta V} = \gamma\kappa. \quad (42)$$

5 The contribution coming from elasticity is more subtle,
6 since the elastic energy is defined in the bulk, while our
7 wish is to define a surface chemical potential. It turns out
8 that one may express the variation of the elastic energy
9 with respect to the interface shape precisely as an integral
10 over the surface, as written above for the surface energy
11 in equation (40). The calculation is given in details in
12 Section 4, and the desired result of the first variation is
13 given by equation (36). In that section please note that
14 δh used above is equivalent to θ multiplied by the normal
15 vector; actually only normal displacements cause a shape
16 change. The change in chemical potential due to stress is
17 thus given by

$$\Delta\mu_e = -\frac{1}{2} [A\varepsilon(u_1) : \varepsilon(u_1) - A\varepsilon(u_2) : \varepsilon(u_2)] \\ + p [\text{div}(u_1) - \text{div}(u_2)] \quad (43)$$

18 where we recall that u_i ($i = 1, 2$) is the displacement field
19 in medium i (see Fig. 3), ε is the deformation (or strain)
20 tensor given by $\varepsilon(u) = (\nabla u + \nabla u^T)/2$, and A is the fourth
21 order tensor which enters Hooke's law, namely the stress
22 tensor σ is related to the deformation by $\sigma = A\varepsilon$ ($A_{ijkl} =$
23 $\lambda\delta_{ik}\delta_{jl} + \mu\delta_{il}\delta_{jk}$ where λ and μ are the Lamé coefficients).
24 Finally p is a Lagrange multiplier introduced in Section 4,
25 and plays the role of a pressure like term of the thin fluid
26 layer, but it must be solved for in a consistent manner, as
27 we have seen in Section 4. We have seen that only in the
28 linear regime p coincides with the load g .

29 Note that if there was only one solid bounded by vac-
30 uum, or by a liquid, then the chemical potential would
31 simply be given by

$$\Delta\mu_e = \frac{1}{2} A\varepsilon(u) : \varepsilon(u) \quad (44)$$

32 as has been used in other contexts (see for example [14]).

33 Once the total chemical potential is obtained one can
34 relate it to the kinetics of the interface. The most sim-
35 ple example is that the normal velocity is proportional to
36 minus the chemical potential drop across the interface.

37 The surface evolution equation (at global equilibrium,
38 as is the case in this problem) – or more precisely the
39 normal velocity of the interface – vanishes if the chemical
40 potential difference vanishes, or equivalently if the energy
41 derivative with respect to the shape vanishes. The second

42 variation of the energy with respect to the interface shape
43 (which is computed in this paper) is proportional to the
44 variation of the chemical potential $\Delta\mu$. It is the second
45 variation of energy with respect to the shape that carries
46 information on stability.

47 There are three major physical effects that drive the
48 surface evolution: (i) if the interface is in contact with
49 a reservoir of a liquid containing the molecules of the
50 solid, and if one disregards diffusion (say if the attache-
51 ment/detachment at the surface is the limiting mecha-
52 nism), then the normal velocity is proportional to the
53 chemical potential difference between two states (say the
54 actual one and the initially flat one), this is the case
55 treated in reference [14], (ii) if the surface dynamics
56 evolves due to surface diffusion (as is probably the case
57 for stylolites), then the surface velocity is proportional to
58 the minus of the Laplacian of the chemical potential drop
59 across the interface $\Delta\mu_T$. This is the case treated in Asaro-
60 Tiller [3], and Yang and Srolovitz [34]. The conclusion
61 about stability is the same in both cases, the difference
62 is encoded in the proportionality pre-factor (which has
63 the same sign in both cases) between the normal velocity
64 and the second derivative of the energy with respect to the
65 shape. (iii) Finally if diffusion in the bulk is included, then
66 the normal velocity will be given by an integral equation,
67 and the Kernel of the integral operator, is proportional to
68 $\Delta\mu_T$ times a propagator (Green's function). The propaga-
69 tor expresses the fact that the dynamics becomes nonlocal
70 (addition of mass at some point at the surface is felt by
71 the molecules in the solution at a distant point-due to
72 depletion-inducing thus a nonlocal self-interaction of the
73 moving boundary). But in all the three cases, the insta-
74 bility is encoded in the sign of the second derivative of the
75 energy (with respect to the interface shape). Of course the
76 precise way the instability evolves later in time, depends
77 on the kinetic mechanisms, but not the existence of the
78 instability itself.

5.4 Instability of solid-solid interfaces: application to stylolites

81 Solid-solid interface roughening has also been studied,
82 e.g. [1,12], where the two solids have different elastic mod-
83 uli. There, it was demonstrated that an instability can
84 emerge only if the two solids have different material prop-
85 erties. This markedly differs from our situation where the
86 instability does occur even when the two solids have identi-
87 cal elastic properties. This is traced back to the very differ-
88 ence of the two models: in our case it is the thin fluid layer
89 that transmits the stresses and materializes the interface,
90 while in [12], the interface notion loses its meaning if the
91 two solids have identical material properties (Eqs. (22)
92 and (23) in [12] implies that the elastic energy vanishes
93 exactly for $\chi = 1$, i.e. for identical material properties).

94 The present model considers a geometry which is close
95 to that of a natural stylolite, where the interface sepa-
96 rates two pieces of rock, and is a medium of dissolution in
97 a fluid phase. Quantitative measurements on stylolite sur-
98 faces, using a high resolution profilometer, demonstrate

that roughening do occur at all scales [27]. The interpretation of this observation is still controversial. It has been proposed that the roughening may be driven by a quenched noise initially present in the rock [6,27]. Here, we propose an alternative mechanism: stylolite might be inherently unstable, and the roughening could be driven by local gradients of strain energy. This interpretation is supported by the observation that stylolite do roughen even in very pure rocks such as chalk, where the amount of heterogeneities (quenched noise) is very low. However, further studies, together with laboratory experiments (mimicking the phenomenon) are needed before drawing more conclusive answers.

6 Conclusion

We have shown that a normal load on a solid-fluid-solid interface leads to an instability when using a boundary condition of transmission of the normal stress, but not the shear stress, across the interface. We have shown both explicitly (from linear theory with regard to the perturbation of a flat interface) and from a more general consideration (still within linear perturbation, but without having resort to an explicit solution of the elastic field) that the flat interface is unstable.

When comparing the final state corresponding to a modulated surface with the initial state having a flat surface, we have shown that the modulated surface has lower energy. Given this fact, and the fact related to the Asaro-Tiller-Grinfeld instability, it is appealing to speculate that this should be the case in an arbitrary geometry and arbitrary boundary conditions, provided that locally the considered moving interface possesses a non zero deviatoric stress component. A mathematical general proof is still lacking.

It must be kept in mind that the present study has introduced two simplifications. (i) The instability wavelength is small as compared with the lateral extent of the interface. This holds for natural interfaces that can be found in rocks, for example stylolites. If it occurs (in some special situation) that this is not the case, then one has to consider the role of lateral boundaries as well. (ii) We have considered a uniaxial stress and not a bi-axial one as occurs in realistic situations. Extensions to more general biaxial pre-stress would be interesting.

Finally, our study has focused on the birth of instability and on the lengthscales that are likely to grow first. Nonlinear effects should become decisive in the course of time as linear theory tells us that the amplitude should grow exponentially with time. How would the final state (if any) look like? How would coarsening (if any) occur, in that how fast is it? These question require a numerical study, and an appropriate way would be to make use of a phase-field model, like in [15].

We acknowledge financial support from the French ministry of research (PPF Dynamique des Systèmes Complexes). The support of Région Rhône Alpes (project Elasticité et Nanostruc-

tures) and of the ANR project Géocarbone are also gratefully acknowledged.

Appendix A: Proof of formula (36)

We first recall that the local derivatives u'_i are x -periodic on Γ_V and that $u'_1 \equiv 0$ on Γ_B . Taking the shape derivative (29) of the expression (27) of the objective functional, we obtain

$$J(\Gamma)' \theta = - \int_{\Omega_i} A \varepsilon(u_i) : \varepsilon(u'_i) - \frac{1}{2} \int_{\partial \Omega_i} A \varepsilon(u_i) : \varepsilon(u_i) \theta n_i.$$

Integrating by parts and using the fact that θ vanishes on the boundaries but on Γ shows that

$$J(\Gamma)' \theta = - \int_{\Gamma} A \varepsilon(u_i) n_i u'_i - \int_{\Gamma_T} g n_2 u'_2 - \frac{1}{2} \int_{\Gamma} A \varepsilon(u_i) : \varepsilon(u_i) \theta n_i.$$

On the other hand, taking the shape derivative (30) of (28) yields

$$J(\Gamma)' \theta = \frac{-1}{2} \int_{\Gamma_T} g n_2 u'_2.$$

Combining the two previous expressions we obtain

$$\begin{aligned} J(\Gamma)' \theta &= \int_{\Gamma} A \varepsilon(u_i) n_i u'_i + \frac{1}{2} \int_{\Gamma} A \varepsilon(u_i) : \varepsilon(u_i) \theta n_i \\ &= \int_{\Gamma} p n_i u'_i + \frac{1}{2} \int_{\Gamma} A \varepsilon(u_i) : \varepsilon(u_i) \theta n_i. \end{aligned} \quad (45)$$

To eliminate the local derivatives in the above equality, we take the shape derivative of the constraint on the displacements, which is conveniently rewritten

$$\int_{\Gamma} u_i n_i = \int_{\Omega_i} \operatorname{div}(u_i) - \int_{\Gamma_T} u_2 n_2 = 0,$$

and obtain

$$0 = \int_{\Omega_i} \operatorname{div}(u'_i) + \int_{\partial \Omega_i} \operatorname{div}(u_i) \theta n_i - \int_{\Gamma_T} u'_2 n_2.$$

Integrating by parts the first term in the above expression, we arrive at

$$\int_{\Omega_i} u'_i n_i = - \int_{\Gamma} \operatorname{div}(u_i) \theta n_i.$$

Finally, injecting this equality in (45) proves (36).

References

1. E. Jettestuen, L. Angheluta, J. Mathiesen, F. Renard, B. Jamtveit, *Phys. Rev. Lett.* **100**, 096106 (2008)
2. F. Arthaud, M. Mattauer, *Bull. Soc. Géol. Fr.* **11**, 738 (1969)
3. R.J. Asaro, W.A. Tiller, *Met. Trans.* **3**, 1789 (1972)
4. R.G.C. Bathurst, *Carbonate sediments and their diagenesis* (Elsevier, Amsterdam, 1971)
5. J. Bisschop, D.K. Dysthe, *Phys. Rev. Lett.* **96**, 146103 (2006)
6. A. Brouste, F. Renard, J.-P. Gratier, J. Schmittbuhl, *J. Struc. Geol.* **29**, 422 (2007)
7. S.W.J. Den Brok, J. Morel, *Geophys. Res. Lett.* **28**, 603 (2001)
8. H.V. Dunnington, *J. Sed. Petrol.* **24**, 27 (1954)
9. D. Gal, A. Nur, E. Aharonov, *Geophys. Res. Lett.* **25**, 1237 (1998)
10. J.P. Gratier, L. Muquet, R. Hassani, F. Renard, *J. Struc. Geol.* **27**, 89 (2005)
11. M. Grinfeld, *Sov. Phys. Dokl.* **31**, 831 (1986)
12. M.A. Grinfeld, *J. Nonlinear Sci.* **3**, 35 (1993)
13. M.T. Heald, *J. Geol.* **63**, 101 (1955)
14. K. Kassner, C. Misbah, *Europhys. Lett.* **28**, 245 (1994)
15. K. Kassner, C. Misbah, *Europhys. Lett.* **46**, 217 (1999)
16. K. Kassner, C. Misbah, J. Müller, J. Kappey, P. Kohlert, *Phys. Rev. E* **63**, 036117 (2001)
17. R. Kerrich, *Zentrabl. Geol. Paleontol.* **5-6**, 512 (1977)
18. D. Koehn, J. Arnold, A. Malthe-Srenssen, B. Jamtveit, *Am. J. Sci.* **303**, 656 (2003)
19. D. Koehn, D.K. Dysthe, B. Jamtveit, *Geochim. Cosmochim. Acta* **68**, 3317 (2004)
20. D.L. Landau, E.M. Lifchitz, *Theory of elasticity*, Butterworth Heinemann (Oxford, UK, 1999)
21. C. Misbah, F. Renard, J.-P. Gratier, K. Kassner, *Geophys. Res. Lett.* **31**, L06618 (2004)
22. F. Murat, J. Simon, *Sur le contrôle par un domaine géométrique*, Rapport du Laboratoire d'Analyse Numérique, 189, 76015. Université de Paris 6, Paris (1976)
23. P. Nozieres, *The grinfield instability of stressed crystals*, in *NATO Ad-vanced Research Workshop on Spatio-Temporal Patterns in Nonequilibrium Complex Systems*, edited by P.E. Cladis, P. Palffy-Muhoray, Vol. 21, 1994
24. W.C. Park, E.H. Schot, *J. Sedimentary Petrology* **38**, 175 (1968)
25. L.B. Railsback, L.M. Andrews, *J. Struc. Geol.* **17**, 911 (1995)
26. F. Renard, J. Schmittbuhl, J.P. Gratier, P. Meakin, E. Merino, *J. Geophys. Res.* **108**, B03209 (2004)
27. J. Schmittbuhl, F. Renard, J.P. Gratier, R. Tous-saint, *Phys. Rev. Lett.* **93**, 238501 (2004)
28. J. Simon, Second variations for domain optimization problems, in *4th International conference on control of distributed parameter systems*, International Series, edited by F. Kappel, K. Kunish, W. Schappacher, Birkhauser, Berlin, 1989
29. J. Simon, *Diferenciacion de problemas de con-torno respecto del dominio*, lecture notes available at <http://wwwlma.univ-bpclermont.fr/~simon/pagePubs.html#vardomaine>. Departamento de An'alisis Matem'atico, Universidad de Sevilla, Sevilla (1991)
30. H.C. Sorby, *Proc. Royal Soc. London* **12**, 538 (1863)
31. D.J. Srolovitz, *Acta Metall.* **37**, 621 (1989)
32. P.B. Stockdale, *Stylolites: Their nature and origin*, Ph.D. thesis, Indiana University Studies, 1922
33. R.H. Torii, S. Balibar, *J. Low Temp. Phys.* **89**, 391 (1992)
34. W.H. Yang, D.J. Srolovitz, *Phys. Rev. Lett.* **71**, 1593 (1993)